

Emergent Superconductivity and Competing Charge Orders in Hole-Doped Square-Lattice t - J Model

Xin Lu,^{1,*} Feng Chen,^{2,*} W. Zhu,³ D. N. Sheng,^{2,†} and Shou-Shu Gong^{1,4,‡}

¹*School of Physics, Beihang University, Beijing 100191, China*

²*Department of Physics and Astronomy, California State University Northridge, California 91330, USA*

³*School of Science, Westlake University, Hangzhou 310024, China, and*

Institute of Natural Sciences, Westlake Institute of Advanced Study, Hangzhou 310024, China, and
Key Laboratory for Quantum Materials of Zhejiang Province, Westlake University, Hangzhou 310024, China

⁴*School of Physical Sciences, Great Bay University, Dongguan 523000, China*

(Dated: April 11, 2023)

Recent large-scale numerical simulations on the square-lattice t - J model demonstrate unconventional d -wave superconductivity on the electron-doped side but a dominant charge density wave (CDW) order on the hole-doped side, which is inconsistent with the high- T_c superconductivity of hole-doped cuprate compounds. To address this issue, we systematically study the square-lattice t - J model with a moderate ratio of the next-nearest-neighbor (t_2) to the nearest-neighbor (t_1) electron hopping t_2/t_1 modeling electron-doped ($t_2 > 0$) and hole-doped ($t_2 < 0$) cuprates, by employing the state-of-the-art density matrix renormalization group calculations. On 6-leg cylindrical system, while different CDW phases are identified on the hole-doped side for the doping range $\delta = 1/16 - 1/8$, a superconducting (SC) phase emerges at lower doping regime, where the pairing correlations exhibit a power-law decay with d -wave symmetry. On the wider 8-leg system, the d -wave SC also emerges on the hole-doped side at the optimal $1/8$ doping, demonstrating a change of the ground-state nature by increasing system width. Our results highlight rich possibilities for the emergence of superconductivity in the general t - J model through weakening the competing charge orders, which could lead to a unified understanding of both hole- and electron-doped cuprate superconductors.

Introduction.— Understanding the unconventional superconductivity (SC) in cuprate systems is a major theme of condensed matter physics [1, 2], which is usually studied in theory based on the square-lattice Hubbard model (large U) and its cousin t - J model [1–8]. Soon after the experimental discovery of cuprate superconductors, the resonating valence bond theory [3] was proposed to describe unconventional SC in these strongly correlated models, which has stimulated intense theoretical explorations [6–14]. However, it remains illusive if these strongly correlated models can capture the main physics of the unconventional superconductivity discovered in cuprate compounds. While analytical solutions are less controlled, numerical studies in the relevant regime [15–46] are also extremely difficult in determining the ground state due to the extensive entanglement and low-energy excitations associated with competing spin and charge degrees of freedom. In recent years, numerical simulations have reached a possible consensus on the ground states of the pure large- U Hubbard and t - J models near the optimal doping, which are the stripe phase [15–28] characterized by a charge density wave (CDW) with π -phase shifted antiferromagnetic domains, accompanied by exponentially decaying SC correlation.

On the other hand, the topology of Fermi surface identified experimentally for the cuprates indicates the importance of a small next-nearest-neighbor (NNN) hopping t_2 [47], with the sign of t_2 modeling the hole- ($t_2 < 0$) and electron-doped ($t_2 > 0$) cuprates, respectively [48]. To explore the role of the NNN hopping in tuning the interplay among different orders, numerical studies on 4-leg Hubbard and t - J models find that introducing either positive or negative t_2 can lead to the coexistence of quasi-long-range SC and CDW orders [35–38]. To improve our understanding of how these orders evolve to-

wards two dimensions (2D), recent density matrix renormalization group (DMRG) studies on the 6- and 8-leg t_1 - t_2 - J models (with $t_1 > 0$) have identified a robust d -wave SC with suppressed CDW at $t_2 > 0$ [39–41], giving insights into the SC of electron-doped cuprates. However, for $t_2 < 0$, the stripe order appears to win over SC near the optimal doping [39, 42, 49], in sharp contrast with the phase diagram of hole-doped cuprates [50]. Nonetheless, DMRG calculations on the t_1 - t_2 - J model also find hole binding in the stripe phase [39, 49], suggesting local hole pairing without longer distance phase coherence. These results indicate that the true nature of the ground state of the hole-doped t - J model with $t_2 < 0$ has not been settled.

In this Letter, we study the quantum phase diagram of hole-doped t - J model and examine the interplay between SC and CDW orders through extensive and accurate DMRG calculations. By tuning doping level δ and hopping ratio t_2/t_1 , we identify the dominance of CDW phases in the hole-doped 6-leg system at $\delta = 1/16 - 1/8$, accompanied by exponentially decaying SC correlation. However, SC and a weak CDW can coexist on the 6-leg system at lower doping region with $\delta = 1/24 - 1/36$ [Fig. 1(a)], where the pairing correlations show the d -wave symmetry and slow power-law decay with the exponent $K_{sc} \lesssim 1$. Importantly, we observe prevalent SC at the optimal doping ($\delta = 1/8$) on an 8-leg cylinder [Fig. 1(b)]. On the electron-doped side ($t_2 > 0$), we confirm the existence of a robust uniform d -wave SC phase in agreement with previous studies [39, 42]. On the hole-doped side ($t_2 < 0$), we observe the emergence of SC with weak or vanishing CDW order, with power-law decaying pairing correlations ($K_{sc} < 2$). Our work suggests that the t - J model may offer a unified framework for understanding the uncon-

ventional SC for both electron- and hole-doped cuprates.

Model and method.— The Hamiltonian of the extended t - J model is defined as

$$H = - \sum_{\{ij\},\sigma} t_{ij} (\hat{c}_{i,\sigma}^\dagger \hat{c}_{j,\sigma} + \text{H.c.}) + \sum_{\{ij\}} J_{ij} (\hat{\mathbf{S}}_i \cdot \hat{\mathbf{S}}_j - \frac{1}{4} \hat{n}_i \hat{n}_j),$$

where $\hat{c}_{i\sigma}^\dagger$ ($\hat{c}_{i\sigma}$) is the creation (annihilation) operator of the electron with spin σ ($\sigma = \pm 1/2$) on site $i = (x_i, y_i)$, $\hat{\mathbf{S}}_i$ is the spin-1/2 operator and $\hat{n}_i = \sum_{\sigma} \hat{c}_{i\sigma}^\dagger \hat{c}_{i\sigma}$ is the electron number operator. The Hilbert space for each site is constrained by no double occupancy ($n_i \leq 1$). We consider the NN and NNN hoppings (t_1 and t_2) and spin superexchange interactions (J_1 and J_2). We choose $J_1 = 1.0$ and set $t_1/J_1 = 3.0$ to make a connection to the corresponding Hubbard model with $U/t = 12$ [51]. The length and width of the square lattice are L_x and L_y , giving the total site number $N = L_x \times L_y$. The doping ratio δ is defined as $\delta = N_h/N$, where N_h is the number of doped holes. We focus on the doping regime $1/36 \leq \delta \leq 1/8$ on 6-leg cylinder and $\delta = 1/8$ on 8-leg cylinder, and tune t_2/t_1 with the fixed relation $(t_2/t_1)^2 = J_2/J_1$ [40, 41].

We solve the ground state of the system by DMRG [52] calculations with $SU(2) \otimes U(1)$ symmetry implemented [53]. We study cylindrical systems with open and periodic boundary conditions along the axial (x) and circumference (y) directions respectively, and keep the bond dimensions of $SU(2)$ multiplets up to $D = 15000$ for 6-leg and 28000 for 8-leg systems, equivalent to about 45000 and 84000 $U(1)$ states respectively, which ensure accurate results with the truncation error less than 1.2×10^{-6} for 6-leg and 2.5×10^{-5} for 8-leg systems (see Supplemental Materials (SM) for more details [54]).

Quantum phase diagram.— Our results are summarised in the phase diagram Fig. 1 as a function of hopping ratio t_2/t_1 and doping level δ . For the 6-leg system with $-0.22 \leq t_2/t_1 \leq 0$ [Fig. 1(a)], we identify two charge ordered phases carrying distinct wavevectors: the stripe phase with wavevector $Q = (3\pi\delta, 0)$ and a W_y3 CDW phase with $Q = (6\pi\delta, 2\pi/3)$ (see SM for the results of the W_y3 CDW state [54]), which shares the similar charge density distribution of the W3 phase found in a previous study of the t_1 - t_2 - J model at hole doping [39]. Strikingly, in the doping regime below $\delta = 1/18$, we discover a quasi-long-range SC order ($K_{sc} \lesssim 1$) coexisting with a weak CDW. Such a low doping regime falls outside the scope of most previous studies.

For the 8-leg system with $-0.2 \leq t_2/t_1 \leq 0.3$ at $\delta = 1/8$ [Fig. 1(b)], a robust d -wave SC order emerges for $t_2/t_1 \gtrsim 0.12$ with a uniform charge density distribution and exponentially decaying single-particle and spin correlations, which is similar to the uniform SC phase identified on 6-leg cylinder [41]. This uniform SC phase may extend to the larger t_2/t_1 regime [55] and persist in 2D limit. Remarkably, the quasi-long-range SC order is also observed on the hole-doped side for $t_2/t_1 \lesssim -0.05$, which exhibits a very weak or vanishing charge order. The SC power exponent $K_{sc} < 2$ indicates a divergent superconducting susceptibility at zero-temperature limit. This result contradicts a previous work studying a sim-

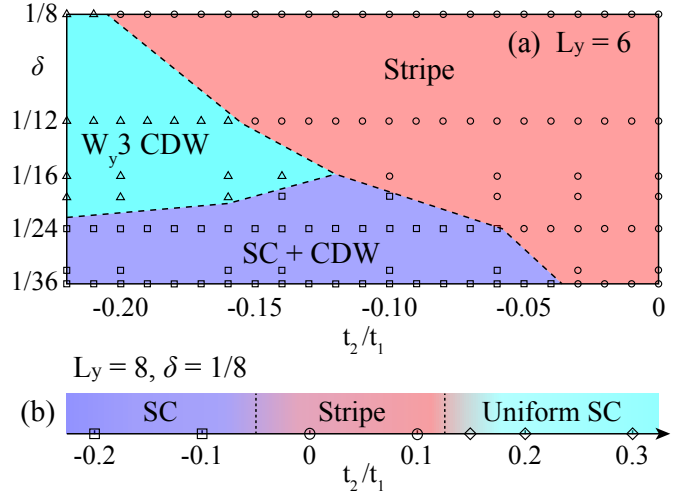


FIG. 1. Quantum phase diagrams of the t_1 - t_2 - J_1 - J_2 model on different system widths. (a) Quantum phase diagram of the $L_y = 6$ cylinder in the range of $-0.22 \leq t_2/t_1 \leq 0$ and $1/36 \leq \delta \leq 1/8$. We identify a stripe phase, a W_y3 CDW phase, and a SC + CDW phase with coexistent d -wave SC and a weak CDW. (b) Quantum phase diagram of the $L_y = 8$ cylinder with $-0.2 \leq t_2/t_1 \leq 0.3$ at $\delta = 1/8$ with two superconducting phases, and a stripe phase in between. The hole-doped SC phase ($t_2/t_1 \lesssim -0.05$) has weak or vanishing CDW order. The symbols denote the parameter points that we have calculated. $(t_2/t_1)^2 = J_2/J_1$ is fixed with tuning parameter.

ilar model without J_2 term that claims the absence of SC in the hole-doped regime [39], which may be attributed to the existence of competing charge ordered states in low energy regime. In our calculation, extremely large bond dimensions are used for reaching convergence and identifying the emergence of SC. For both 6- and 8-leg systems at hole doping, superconductivity emerges through suppressing charge order as we demonstrate below.

SC pairing correlation.— We examine SC by the dominant spin-singlet pairing correlations $P_{\alpha,\beta}(\mathbf{r}) = \langle \hat{\Delta}_\alpha^\dagger(\mathbf{r}_0) \hat{\Delta}_\beta(\mathbf{r}_0 + \mathbf{r}) \rangle$, where the pairing operator is defined as $\hat{\Delta}_\alpha(\mathbf{r}) = (\hat{c}_{\mathbf{r}\uparrow} \hat{c}_{\mathbf{r}+\mathbf{e}_\alpha\downarrow} - \hat{c}_{\mathbf{r}\downarrow} \hat{c}_{\mathbf{r}+\mathbf{e}_\alpha\uparrow}) / \sqrt{2}$ and $\mathbf{e}_{\alpha=x,y}$ denote the unit vectors along the x and y directions. Since the wave function in DMRG calculation is represented as a matrix product state, correlation functions usually decay exponentially at finite bond dimensions [57]. We carefully make the bond dimension scaling to demonstrate the true nature of correlations at $D \rightarrow \infty$ (see Fig. 2 and SM [54]).

We first compare the pairing correlations of different phases on 6-leg systems. In the stripe phase represented by $t_2/t_1 = -0.06$ and $\delta = 1/12$ [Fig. 2(a)], the pairing correlation $P_{yy}(r)$ grows smoothly with bond dimension and follows an exponential decay $P_{yy}(r) \sim \exp(-r/\xi_{sc})$ with $\xi_{sc} \simeq 3.69$ after the extrapolation to $D \rightarrow \infty$. In the SC + CDW phase, as shown in Fig. 2(b) for $t_2/t_1 = -0.08$ at lower doping $\delta = 1/24$, $P_{yy}(r)$ increases drastically compared with that in the stripe phase and exhibits an algebraic decay $P_{yy}(r) \sim r^{-K_{sc}}$ with $K_{sc} \simeq 0.82$, characterizing a quasi-

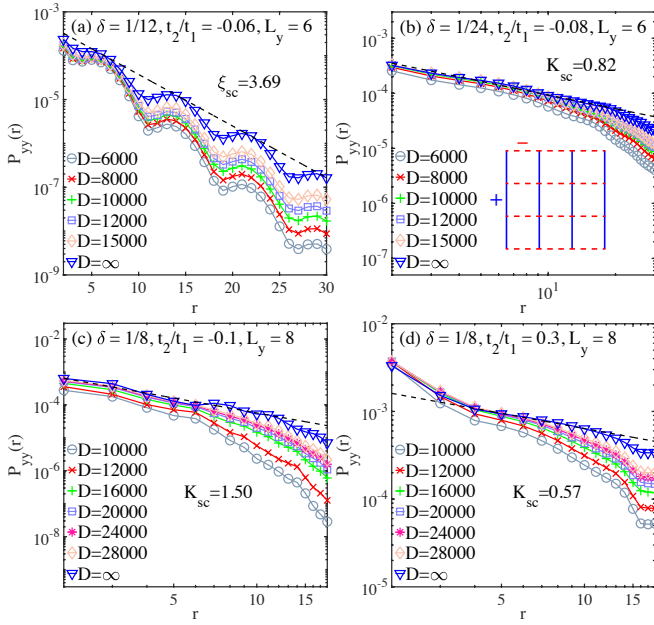


FIG. 2. SC pairing correlation functions. (a) Semi-logarithmic plot of pairing correlation $P_{yy}(r)$ at different bond dimensions in the stripe phase at $L_y = 6$. The correlation length ξ_{sc} is obtained by fitting the function $P_{yy}(r) \sim \exp(-r/\xi_{sc})$. (b) Double-logarithmic plot of $P_{yy}(r)$ in the SC + CDW phase on 6-leg cylinder. The dash line represents the fitting of the extrapolated data at $D \rightarrow \infty$ with $P_{yy}(r) \sim r^{-K_{sc}}$. The power exponent $K_{sc} \simeq 0.82$ characterizes a quasi-long-range SC order. The inset shows the signs of SC order for the d -wave symmetry. (c) and (d) are the similar plots of $P_{yy}(r)$ in the hole-doped SC ($t_2 < 0$) and uniform d -wave SC phases ($t_2 > 0$) on 8-leg cylinder, both with the power exponents $K_{sc} < 2$ indicating the divergence of SC susceptibility [56].

long-range SC order. The divergent SC susceptibility corresponding to $K_{sc} < 2$ [56] is a universal feature within this SC + CDW phase on 6-leg system. We also confirm that other kinds of pairing correlations have the same magnitudes, i.e. $P_{yy}(r) \simeq -P_{yx}(r) \simeq P_{xx}(r)$, in accordance with d -wave symmetry as illustrated in the inset of Fig. 2(b) rather than the plaquette d -wave symmetry found in the 4-leg Hubbard model at $t_2 < 0$ [37].

To further investigate whether SC can emerge on a wider system at $t_2 < 0$, we perform extensive simulations on the 8-leg cylinder at the optimal doping $\delta = 1/8$, which is more relevant to the experiments of cuprates. For $t_2/t_1 = -0.1$ on the $N = 24 \times 8$ cylinder [Fig. 2(c)], the pairing correlation $P_{yy}(r)$ at longer distances grows rapidly with bond dimension. The extrapolated results at $D \rightarrow \infty$ can be fitted by a power-law decay with $K_{sc} \simeq 1.5$, demonstrating an emergent quasi-long-range SC order. We also present the pairing correlation in the uniform SC phase at $t_2 > 0$, as shown in Fig. 2(d) for $t_2/t_1 = 0.3$, which exhibit a slow algebraic decay with a small exponent $K_{sc} \simeq 0.57$ characterizing a robust SC phase.

Charge density distribution.— The charge density distributions in the stripe, SC + CDW, SC, and uniform d -wave SC phases are usually uniform along the y direction, and

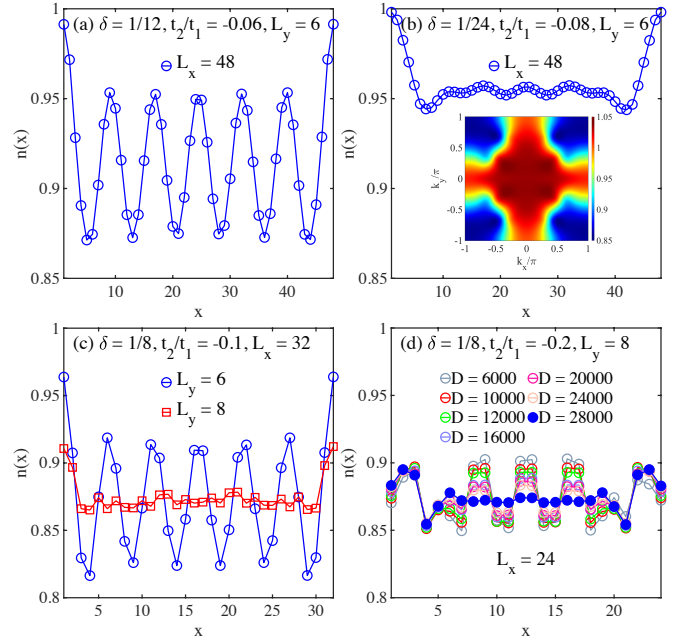


FIG. 3. Charge density profiles. The charge density distributions $n(x) = \frac{1}{L_y} \sum_{y=1}^{L_y} \langle \hat{n}_{x,y} \rangle$ in (a) stripe phase and (b) SC + CDW phase on the 6-leg cylinder with $L_x = 48$. The inset of (b) shows the corresponding electron momentum distribution $n(\mathbf{k})$ obtained from the middle 24×6 sites. (c) Comparing $n(x)$ in the SC phase on 8-leg cylinder and the stripe phase on 6-leg cylinder, for the same $t_2/t_1 = -0.1$, $\delta = 1/8$, and $L_x = 32$. The results are obtained at $D = 15000$ and 24000 for $L_y = 6$ and 8 , respectively. (d) $n(x)$ in the SC phase of 8-leg cylinder with $t_2/t_1 = -0.2$, $\delta = 1/8$, and $L_x = 24$ obtained at different bond dimensions.

we show the averaged charge density for each column as $n(x) = \sum_{y=1}^{L_y} \langle \hat{n}_{x,y} \rangle / L_y$ in Fig. 3. For 6-leg system, we find the CDW wavelength $\lambda \simeq 4/(L_y\delta)$ in the stripe phase [Fig. 3(a)], corresponding to four holes on average for each CDW unit. In the SC + CDW phase, the CDW wavelength $\lambda \simeq 2/(L_y\delta)$ indicates two holes in each CDW unit [Fig. 3(b)]. Significantly, one can see that here the oscillation amplitude of $n(x)$ (i.e. charge order) is much weaker than that in the stripe phase shown in Fig. 3(a) (about 20 times smaller). We also present the momentum distribution $n(\mathbf{k}) = \frac{1}{N} \sum_{i,j,\sigma} \langle \hat{c}_{i,\sigma}^\dagger \hat{c}_{j,\sigma} \rangle e^{i\mathbf{k} \cdot (\mathbf{r}_i - \mathbf{r}_j)}$ in the SC + CDW phase [in the inset of Fig. 3(b)]. The unenclosed Fermi surface topology around $\mathbf{k} = (\pm\pi, 0)$ and $(0, \pm\pi)$ is consistent with that observed in the ARPES measurement of hole-doped cuprates [47, 58, 59], and is distinctly different from the topology for electron doping at $t_2 > 0$ [39, 41], where the Fermi surface forms a closed pocket around $\mathbf{k} = (0, 0)$.

A natural question is how the charge order evolves towards 2D limit. Crucially, we find that the strong CDW in the stripe phase at $t_2 < 0$ for $L_y = 6$ can be significantly suppressed on wider system, with evidence shown in Fig. 3(c) for a comparison between $L_y = 6$ and 8 systems at $t_2/t_1 = -0.1$. The quite weak charge density oscillation on the 32×8 system is similar to that of the SC + CDW phase on 6-leg cylin-

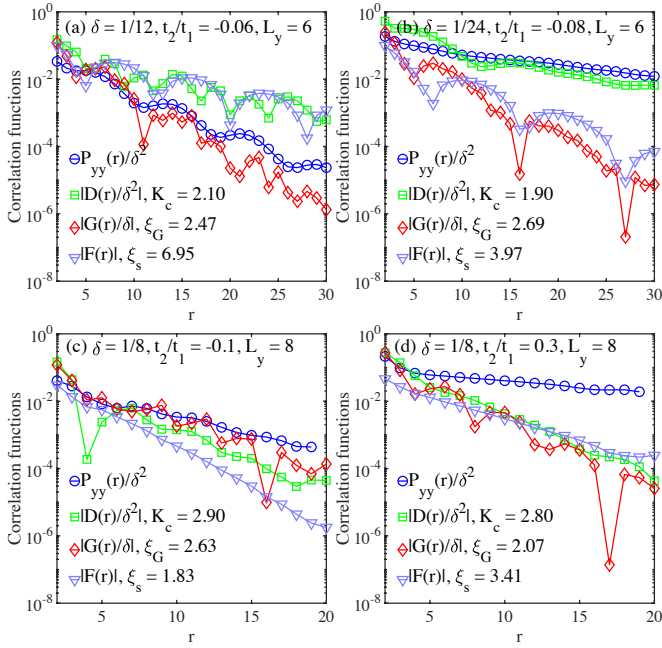


FIG. 4. Correlations in the stripe and superconducting phases. The presented data are those after the extrapolation to $D \rightarrow \infty$. Comparison among pairing correlation $P_{yy}(r)$, charge density correlation $D(r)$, single-particle Green's function $G(r)$, and spin correlation $F(r)$ for (a) stripe phase at $L_y = 6$, (b) SC + CDW phase at $L_y = 6$, (c) hole-doped SC phase at $L_y = 8, \delta = 1/8$, and (d) uniform d -wave SC phase at $L_y = 8, \delta = 1/8$. The correlations are rescaled by δ to make a direct comparison. The power exponent K and correlation length ξ are obtained by fitting these correlations as power-law and exponential decay, respectively. The fitting details can be found in SM [54].

der [Fig. 3(b)]. The weakened or vanishing charge order for $L_y = 8$ is accompanied with the emergent quasi-long-range SC order shown in Fig. 2(c). In Fig. 3(d), we show the evolution of charge density profile for $t_2/t_1 = -0.2$ deep in the SC phase. One can find the charge distribution is gradually transformed from a CDW-like pattern to a nearly uniform one with increasing bond dimension, demonstrating extremely weak or vanishing charge order in the hole-doped SC phase and the importance of large bond dimensions for reaching the true ground state (see SM for additional examples [54]).

Correlation functions.— In Fig. 4, we further compare various correlation functions in the different phases on 6- and 8-leg cylinders. While all the correlations are demonstrated in semi-logarithmic scale, the exponents K and ξ are obtained by power-law and exponential fittings, respectively [54]. For the stripe phase on 6-leg cylinder [Fig. 4(a)], while the single-particle Green's function $G(r) = \langle \sum_{\sigma} \hat{c}_{x,y,\sigma}^{\dagger} \hat{c}_{x+r,y,\sigma} \rangle$ and pairing correlation appear to decay exponentially [54], the intertwined charge density correlation $D(r) = \langle \hat{n}_{x,y} \hat{n}_{x+r,y} \rangle - \langle \hat{n}_{x,y} \rangle \langle \hat{n}_{x+r,y} \rangle$ and spin correlation $F(r) = \langle \mathbf{S}_{x,y} \cdot \mathbf{S}_{x+r,y} \rangle$ are more dominant at longer distances and show the feature of π phase shift. In contrast, in the SC + CDW [Fig. 4(b)], hole-doped SC [Fig. 4(c)], and uniform d -wave SC phases

[Fig. 4(d)], pairing correlation is dominant over other correlations at longer distances. Furthermore, on the 24×8 system, $G(r)$ and $F(r)$ show the exponential decay with short correlation lengths $\xi_G \simeq 2.63$, $\xi_s \simeq 1.83$ and $\xi_G \simeq 2.07$, $\xi_s \simeq 3.41$ for $t_2/t_1 = -0.1$ in the hole-doped SC phase and $t_2/t_1 = 0.3$ in the uniform d -wave SC phase, respectively. The suppressed single-particle and spin correlations are consistent with DMRG results of the same model at larger t_2/t_1 , which correspond to doping either the J_1 - J_2 spin liquid or valence bond solid state [55].

Summary and Discussion.— We have presented a global picture for both the electron-doped ($t_2 > 0$) and hole-doped ($t_2 < 0$) square-lattice t - J model by employing the cutting-edge DMRG calculations. While we confirm the uniform d -wave SC phase for the electron-doped side on wider cylinder which may survive in 2D limit, we find that the ground states of the hole-doped t - J model also can be superconducting, at both the doping regime $\delta = 1/36 - 1/24$ for $L_y = 6$ and the optimal doping $\delta = 1/8$ for $L_y = 8$. In these superconducting phases, the pairing correlations exhibit a power-law decay ($K_{sc} < 2$) with d -wave symmetry. On the hole-doped side at $\delta = 1/8$, superconductivity turns out to be favored on the wider $L_y = 8$ system, where the enhanced phase coherence of the paired holes [49] helps to destabilize CDW order and thus allows superconductivity to develop.

Due to the strong competition between stripe and SC orders at hole doping [39], the obtained ground state may sensitively depend on the convergence of calculation or the NNN spin coupling. By keeping extremely large bond dimensions, we establish the strong suppression of the CDW order on the 8-leg system with a moderate t_2 and J_2 . To sum up, we conclude that the single-band t - J model has some generic features including the uniform superconductivity at electron doping, and the dominant superconductivity with near vanishing or coexisting CDW order at hole doping, which may provide a basic description of the cuprate superconductors.

At last, we discuss some open questions. For hole doping, the charge order with suppressed SC is commonly observed in low-energy excited states or ground states of narrower system ($L_y = 6$) with hole binding [39, 49], which may have some connection with the pseudogap physics [60, 61] of the cuprate system. The d -wave SC on the electron-doped side turns out to be very robust on wider cylinder, however the nature of its spin correlations is still under debate [39, 41]. On finite cylinders ($L_y = 6 - 8$), spin correlations decay exponentially with a short correlation length (ξ_s), but with a slowly decreasing ratio of ξ_s/L_y , which makes it uncertain about how the spin correlation evolves into thermodynamic limit. We hope our work can stimulate more future studies to address these challenging issues.

Acknowledgments.— We thank Zheng-Yu Weng, Steven Kivelson, Hongchen Jiang, and Shengtao Jiang for stimulating discussions. X. L. and S. S. G. were supported by the National Natural Science Foundation of China (Grants No. 12274014 and No. 11834014). W. Z. was supported by National R&D program under No. 2022YFA140220, R&D Program of Zhe-

jiang (2022SDXHDX0005). F. C. and D. N. S. was supported by the U.S. Department of Energy, Office of Basic Energy Sciences under Grant No. DE-FG02-06ER46305 for studying unconventional superconductivity.

Note added.— At the final stage of preparing this work, we have become aware of an independent and related work focusing on the larger positive $t_2/t_1 \simeq 0.7$ regime of the same t - J model on 8-leg cylinder [55], as well as two other works focusing on the Hubbard model [62, 63]. The results in Ref. [55] are consistent with our findings at $t_2/t_1 = 0.3$.

* Both authors contributed equally to this work.

† donna.sheng1@csun.edu

‡ shoushu.gong@buaa.edu.cn

- [1] B. Keimer, S. A. Kivelson, M. R. Norman, S. Uchida, and J. Zaanen, *Nature* **518**, 179 (2015).
- [2] C. Proust and L. Taillefer, *Annual Review of Condensed Matter Physics* **10**, 409 (2019).
- [3] P. W. Anderson, *Science* **235**, 1196 (1987).
- [4] D. P. Arovas, E. Berg, S. A. Kivelson, and S. Raghu, *Annual Review of Condensed Matter Physics* **13**, 239 (2022).
- [5] S. Sachdev, *Rev. Mod. Phys.* **75**, 913 (2003).
- [6] P. W. Anderson, P. A. Lee, M. Randeria, T. M. Rice, N. Trivedi, and F. C. Zhang, *Journal of Physics: Condensed Matter* **16**, R755 (2004).
- [7] P. A. Lee, N. Nagaosa, and X.-G. Wen, *Rev. Mod. Phys.* **78**, 17 (2006).
- [8] M. Ogata and H. Fukuyama, *Rep. Prog. Phys.* **71**, 036501 (2008).
- [9] P. W. Anderson, G. Baskaran, Z. Zou, and T. Hsu, *Phys. Rev. Lett.* **58**, 2790 (1987).
- [10] S. A. Kivelson, D. S. Rokhsar, and J. P. Sethna, *Phys. Rev. B* **35**, 8865 (1987).
- [11] Z. Y. Weng, D. N. Sheng, Y.-C. Chen, and C. S. Ting, *Phys. Rev. B* **55**, 3894 (1997).
- [12] T. Senthil and M. P. A. Fisher, *Phys. Rev. B* **62**, 7850 (2000).
- [13] R. K. Kaul, Y. B. Kim, S. Sachdev, and T. Senthil, *Nature Physics* **4**, 28 (2008).
- [14] Z.-Y. Weng, *New Journal of Physics* **13**, 103039 (2011).
- [15] S. R. White and D. J. Scalapino, *Phys. Rev. Lett.* **80**, 1272 (1998).
- [16] S. R. White and D. J. Scalapino, *Phys. Rev. B* **60**, R753 (1999).
- [17] S. R. White and D. J. Scalapino, *Phys. Rev. Lett.* **91**, 136403 (2003).
- [18] G. Hager, G. Wellein, E. Jeckelmann, and H. Fehske, *Phys. Rev. B* **71**, 075108 (2005).
- [19] P. Corboz, T. M. Rice, and M. Troyer, *Phys. Rev. Lett.* **113**, 046402 (2014).
- [20] J. P. F. LeBlanc, A. E. Antipov, F. Becca, I. W. Bulik, G. K.-L. Chan, C.-M. Chung, Y. Deng, M. Ferrero, T. M. Henderson, C. A. Jiménez-Hoyos, E. Kozik, X.-W. Liu, A. J. Millis, N. V. Prokof'ev, M. Qin, G. E. Scuseria, H. Shi, B. V. Svistunov, L. F. Tocchio, I. S. Tupitsyn, S. R. White, S. Zhang, B.-X. Zheng, Z. Zhu, and E. Gull (Simons Collaboration on the Many-Electron Problem), *Phys. Rev. X* **5**, 041041 (2015).
- [21] G. Ehlers, S. R. White, and R. M. Noack, *Phys. Rev. B* **95**, 125125 (2017).
- [22] B.-X. Zheng, C.-M. Chung, P. Corboz, G. Ehlers, M.-P. Qin, R. M. Noack, H. Shi, S. R. White, S. Zhang, and G. K.-L. Chan, *Science* **358**, 1155 (2017).
- [23] E. W. Huang, C. B. Mendl, S. Liu, S. Johnston, H.-C. Jiang, B. Moritz, and T. P. Devereaux, *Science* **358**, 1161 (2017).
- [24] K. Ido, T. Ohgoe, and M. Imada, *Phys. Rev. B* **97**, 045138 (2018).
- [25] H.-C. Jiang, Z.-Y. Weng, and S. A. Kivelson, *Phys. Rev. B* **98**, 140505 (2018).
- [26] B. Ponsioen, S. S. Chung, and P. Corboz, *Phys. Rev. B* **100**, 195141 (2019).
- [27] M. Qin, C.-M. Chung, H. Shi, E. Vitali, C. Hubig, U. Schollwöck, S. R. White, and S. Zhang (Simons Collaboration on the Many-Electron Problem), *Phys. Rev. X* **10**, 031016 (2020).
- [28] H. Xu, H. Shi, E. Vitali, M. Qin, and S. Zhang, *Phys. Rev. Res.* **4**, 013239 (2022).
- [29] G. B. Martins, J. C. Xavier, L. Arrachea, and E. Dagotto, *Phys. Rev. B* **64**, 180513 (2001).
- [30] S. Sorella, G. B. Martins, F. Becca, C. Gazza, L. Capriotti, A. Parola, and E. Dagotto, *Phys. Rev. Lett.* **88**, 117002 (2002).
- [31] A. Himeda, T. Kato, and M. Ogata, *Phys. Rev. Lett.* **88**, 117001 (2002).
- [32] C. T. Shih, T. K. Lee, R. Eder, C.-Y. Mou, and Y. C. Chen, *Phys. Rev. Lett.* **92**, 227002 (2004).
- [33] S. R. White and D. J. Scalapino, *Phys. Rev. B* **79**, 220504 (2009).
- [34] A. Eberlein and W. Metzner, *Phys. Rev. B* **89**, 035126 (2014).
- [35] J. F. Dodaro, H.-C. Jiang, and S. A. Kivelson, *Phys. Rev. B* **95**, 155116 (2017).
- [36] H.-C. Jiang and T. P. Devereaux, *Science* **365**, 1424 (2019).
- [37] C.-M. Chung, M. Qin, S. Zhang, U. Schollwöck, and S. R. White (The Simons Collaboration on the Many-Electron Problem), *Phys. Rev. B* **102**, 041106 (2020).
- [38] Y.-F. Jiang, J. Zaanen, T. P. Devereaux, and H.-C. Jiang, *Phys. Rev. Research* **2**, 033073 (2020).
- [39] S. Jiang, D. J. Scalapino, and S. R. White, *Proceedings of the National Academy of Sciences* **118**, e2109978118 (2021).
- [40] H.-C. Jiang and S. A. Kivelson, *Phys. Rev. Lett.* **127**, 097002 (2021).
- [41] S. Gong, W. Zhu, and D. N. Sheng, *Phys. Rev. Lett.* **127**, 097003 (2021).
- [42] S. Jiang, D. J. Scalapino, and S. R. White, *Phys. Rev. B* **106**, 174507 (2022).
- [43] A. Wietek, *Phys. Rev. Lett.* **129**, 177001 (2022).
- [44] A. Wietek, Y.-Y. He, S. R. White, A. Georges, and E. M. Stoudenmire, *Phys. Rev. X* **11**, 031007 (2021).
- [45] D.-W. Qu, B.-B. Chen, X. Lu, Q. Li, Y. Qi, S.-S. Gong, W. Li, and G. Su, (2022), [arXiv:2211.06322](https://arxiv.org/abs/2211.06322).
- [46] S. Jiang, D. J. Scalapino, and S. R. White, (2023), [arXiv:2303.00756](https://arxiv.org/abs/2303.00756).
- [47] A. Damascelli, Z. Hussain, and Z.-X. Shen, *Rev. Mod. Phys.* **75**, 473 (2003).
- [48] V. I. Belinicher, A. L. Chernyshev, and V. A. Shubin, *Phys. Rev. B* **53**, 335 (1996).
- [49] X. Lu, J.-X. Zhang, S.-S. Gong, D. N. Sheng, and Z.-Y. Weng, (2023), [arXiv:2303.13498](https://arxiv.org/abs/2303.13498).
- [50] D. J. Scalapino, *Rev. Mod. Phys.* **84**, 1383 (2012).
- [51] K. Misumi, T. Kaneko, and Y. Ohta, *Phys. Rev. B* **95**, 075124 (2017).
- [52] S. R. White, *Phys. Rev. Lett.* **69**, 2863 (1992).
- [53] I. P. McCulloch and M. Gulácsi, *Europhysics Letters* **57**, 852 (2002).
- [54] See supplementary materials for more supporting data.
- [55] H.-C. Jiang, S. A. Kivelson, and D.-H. Lee, (2023), [arXiv:2302.11633](https://arxiv.org/abs/2302.11633).

- [56] E. Arrigoni, E. Fradkin, and S. A. Kivelson, *Phys. Rev. B* **69**, 214519 (2004).
- [57] U. Schollwöck, *Rev. Mod. Phys.* **77**, 259 (2005).
- [58] M. A. Hossain, J. D. F. Mottershead, D. Fournier, A. Bostwick, J. L. McChesney, E. Rotenberg, R. Liang, W. N. Hardy, G. A. Sawatzky, I. S. Elfimov, D. A. Bonn, and A. Damascelli, *Nature Physics* **4**, 527 (2008).
- [59] M. Platié, J. D. F. Mottershead, I. S. Elfimov, D. C. Peets, R. Liang, D. A. Bonn, W. N. Hardy, S. Chiuzbaian, M. Falub, M. Shi, L. Patthey, and A. Damascelli, Fermi surface and quasi-particle excitations of overdoped $\text{tl}_2\text{ba}_2\text{cuo}_{6+\delta}$, *Phys. Rev. Lett.* **95**, 077001 (2005).
- [60] P. A. Lee, *Phys. Rev. X* **4**, 031017 (2014).
- [61] Z. Dai, T. Senthil, and P. A. Lee, *Phys. Rev. B* **101**, 064502 (2020).
- [62] H. Xu, C.-M. Chung, M. Qin, U. Schollwöck, S. R. White, and S. Zhang, (2023), [arXiv:2303.08376](https://arxiv.org/abs/2303.08376).
- [63] Y.-F. Jiang, T. P. Devereaux, and H.-C. Jiang, (2023), [arXiv:2303.15541](https://arxiv.org/abs/2303.15541).

Supplemental Materials for: “Emergent Superconductivity and Competing Charge Orders in Hole-Doped Square-Lattice t - J Model”

In the Supplemental Materials, we provide more numerical results to support the conclusions we have discussed in the main text. In Sec. A, we show the bond dimension scaling of correlation functions in the different phases on 6- and 8-leg cylinders, and analyze the decay exponents of these correlations. In Sec. B, we present the charge density profiles in different phases on 6- and 8-leg cylinders. In particular, we show how the charge density distributions gradually converge with growing bond dimension on 8-leg systems. In Sec. C, we supplement more parameter points for the pairing correlations in the SC + CDW phase on 6-leg cylinder and the hole-doped SC phase on 8-leg cylinder. In Sec. D, we discuss more physical properties of the W_y 3 CDW state. In Sec. E and Sec. F, we demonstrate and analyze the evolution of static spin structure factor $S(\mathbf{k})$ and electron momentum distribution $n(\mathbf{k})$. In Sec. G, we show the details of the extrapolation of correlation functions with increasing bond dimension.

A. Correlation functions on 6- and 8-leg cylinders

In this section, we further discuss the simulation results of various correlation functions on 6- and 8-leg cylinders to provide more supports for the data shown in the main text.

As shown in Fig. S1(a1-d1), we perform the polynomial bond dimension extrapolation (see the details in Section G) for the charge density correlation $D(r)$, spin correlation $F(r)$, and single-particle Green’s function $G(r)$ in the stripe phase on 6-leg cylinder. We keep the bond dimensions up to 15000 SU(2) multiplets (equivalent to about 45000 U(1) states), which lead to a good convergence for our results. For density correlation $D(r)$, we present two ways of plotting as shown in Fig. S1(a1-b1), where the power exponent K_c is slightly larger than 2 in double-logarithmic scale, while it also can be fitted exponentially with $\xi_c \simeq 6.55$. One can find that density correlation is the strongest among the correlations shown in Fig. 4(a). For $F(r)$ [Fig. S1(c1)] and $G(r)$ [Fig. S1(d1)], one can find that these two correlations well follow the exponential decay $\exp(-r/\xi)$, which are consistent with the stripe phase found on the $t_2/t_1 > 0$ side by a previous work [41]. The corresponding correlation lengths are found as $\xi_s \simeq 6.95$, and $\xi_G \simeq 2.47$.

Following the same procedure, we extrapolate the various correlation functions in the SC + CDW phase on 6-leg cylinder as shown in Fig. S1(a2-d2). One can see that both the spin correlation in Fig. S1(c2) and single-particle Green’s function in Fig. S1(d2) are short ranged with $\xi_s \simeq 3.97$ and $\xi_G \simeq 2.69$ respectively. The density correlation in the SC + CDW phase also can be fitted algebraically with $K_c \simeq 1.90$ as shown in Fig. S1(a2), and one can find that the related exponents may not follow the general behavior of the Luther-Emery liquids (i.e. $K_{sc} = 1/K_c$). These results may indicate a crossover of the quasi-long ranged SC order from dominated by the strong quantum fluctuations of one-dimensional system to be more like a two-dimensional (finite size) system. We also try to plot $D(r)$ in semi-logarithmic scale as shown in Fig. S1(b2), which could yield a relatively larger correlation length with $\xi_c \simeq 8.30$. This density correlation has also been compared with the pairing correlation as shown in Fig. 4(b), showing that the density correlation is highly intertwined with the pairing correlation. Hence, we identify the phase where the SC and CDW orders are coexistent as shown in Fig. 1(a).

By the same way, we extrapolate these correlation functions on 8-leg cylinder as shown in Fig. S2. Since the computational complexity increases exponentially with the increase of L_y , we keep the bond dimensions up to 28000 SU(2) multiplets for a good convergence, which are equivalent to about 84000 U(1) states and reach our simulation limit. One can see that in both the hole-doped SC and the uniform d -wave SC phases, the three correlation functions $D(r)$, $F(r)$, and $G(r)$ are well characterized by exponential decay. Although we can always plot the charge density correlations in double-logarithmic scale as shown in Fig. S2(a1), (a2) and (a3), their fitting power exponents are clearly larger than 2. Hence, the charge density correlations do not develop quasi-long-range order due to the non-divergent CDW susceptibility [56]. We also find that $K_c K_{sc} = 1$ is not well satisfied in the two phases.

B. Charge density profiles on 6- and 8-leg cylinders

In the main text, we have pointed out that the charge density waves carry different wavevectors Q in the stripe and SC + CDW phase as shown in Figs. 3(a) and 3(b). Here, in order to demonstrate our conclusions still hold in the thermodynamic limit $L_x \rightarrow \infty$ and exclude the finite-size effect, we try to calculate the charge density distributions for different lattice sizes ($L_x = 24 - 64$) while fixing the doping ratio as shown in Fig. S3. Following the same convention of the main text, the average charge density per column is defined as $n(x) = \frac{1}{L_y} \sum_{y=1}^{L_y} \langle \hat{n}_{x,y} \rangle$, where $\hat{n}_{x,y} = \sum_{\sigma} \hat{c}_{(x,y),\sigma}^{\dagger} \hat{c}_{(x,y),\sigma}$ is the electron number operator defined on the site (x, y) . In Fig. S3(a1-e1), we show the charge density profiles in the stripe phase represented by $t_2/t_1 = -0.06$ and $\delta = 1/12$. One can see that the wavelength for different L_x is always $\lambda \simeq 4/(L_y \delta) = 8$, i.e. $Q = (3\pi\delta, 0)$,

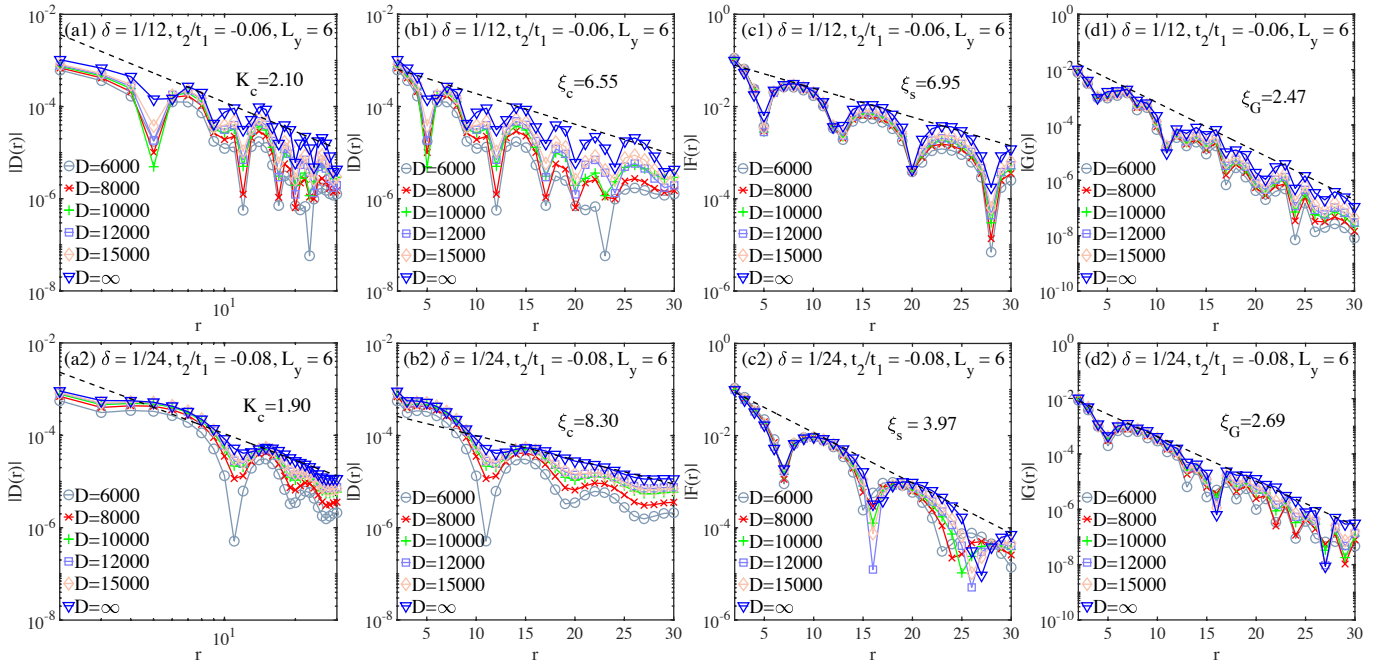


FIG. S1. **Scaling of the correlations in the stripe phase and SC + CDW phase on the $L_y = 6, L_x = 48$ cylinders.** (a1) and (b1) are respectively the double- and semi-logarithmic plots of charge density correlation $D(r)$ obtained by different bond dimensions in the stripe phase. (c1) and (d1) are the semi-logarithmic plots of spin correlation $F(r)$ and single-particle Green's function $G(r)$ in the same phase separately. The dashed line denotes the fitting of the extrapolated $D \rightarrow \infty$ results, where the corresponding power exponent K_c and correlation length ξ are obtained by fitting the algebraic behaviour $D(r) \sim r^{-K_c}$ and exponential behaviour $\sim \exp(-r/\xi)$. (a2-d2) are the similar correlations in the SC + CDW phase.

which remains true for other doping levels in the stripe phase. That is to say, each stripe is filled with four holes, consistent with the CDW phase on the $t_2/t_1 > 0$ side [41]. Similarly, we also show the charge density profiles in the SC + CDW phase as shown in Fig. S3(a2-e2) represented by $t_2/t_1 = -0.08$ and $\delta = 1/24$. Different from the stripe phase, here we identify the wavelength is matched with $\lambda \simeq 2/(L_y \delta) = 8$, i.e. $Q = (6\pi\delta, 0)$. Such a pattern of two holes filled in each stripe has also been observed in the SC + CDW phase on the 6-leg cylinder system with $t_2/t_1 > 0$ [41]. Here, the truncation errors for all the simulations are about $\mathcal{O}(10^{-6})$ to ensure full convergence of the measurements.

In Figs. 3(c) and 3(d), we have also shown the charge density profiles in the hole-doped SC phase on 8-leg cylinders, which have quite weak charge density oscillations (static charge order). Here we further show the evolution of charge density profile with growing bond dimension in Fig. 3(d) for a better visualization, as shown in Fig. S4. One can see that the charge density distributions are not uniform along the circumference (y) direction at lower bond dimensions D , which is repaired with growing bond dimension and the CDW pattern is gradually suppressed.

In Fig. S5(a), we show another example of the evolution of charge density profile in the hole-doped SC phase on 8-leg cylinder, with $t_2/t_1 = -0.1$. One can see that the CDW is robust below $D = 12000$, while it sharply becomes weak around $D = 16000$. We also show the same trend in the uniform d -wave SC phase [Fig. S5(b)] with growing bond dimension. The nearly flat charge density distribution indicates the same nature as that of the 6-leg uniform d -wave SC phase found at $t_2/t_1 > 0$ side [41].

C. Pairing correlation functions for more parameter points in the superconducting phases

Here we show the pairing correlations for more parameter points to support the superconducting phase region demonstrated in the phase diagram. We first provide another representative point at $\delta = 1/36, t_2/t_1 = -0.08$. In Fig. S6(a), one can see that the pairing correlation $P_{yy}(r)$ can be fitted algebraically with $K_{sc} \simeq 1.01$ after bond dimension extrapolation. For the hole-doped SC phase on 8-leg cylinder, we also show the scaling of pairing correlations at $\delta = 1/8, t_2/t_1 = -0.2$ [Fig. S6(b)], where the extrapolated $P_{yy}(r)$ can also be fitted algebraically with $K_{sc} \simeq 1.63$. These results are consistent with the phase diagram presented in the main text.

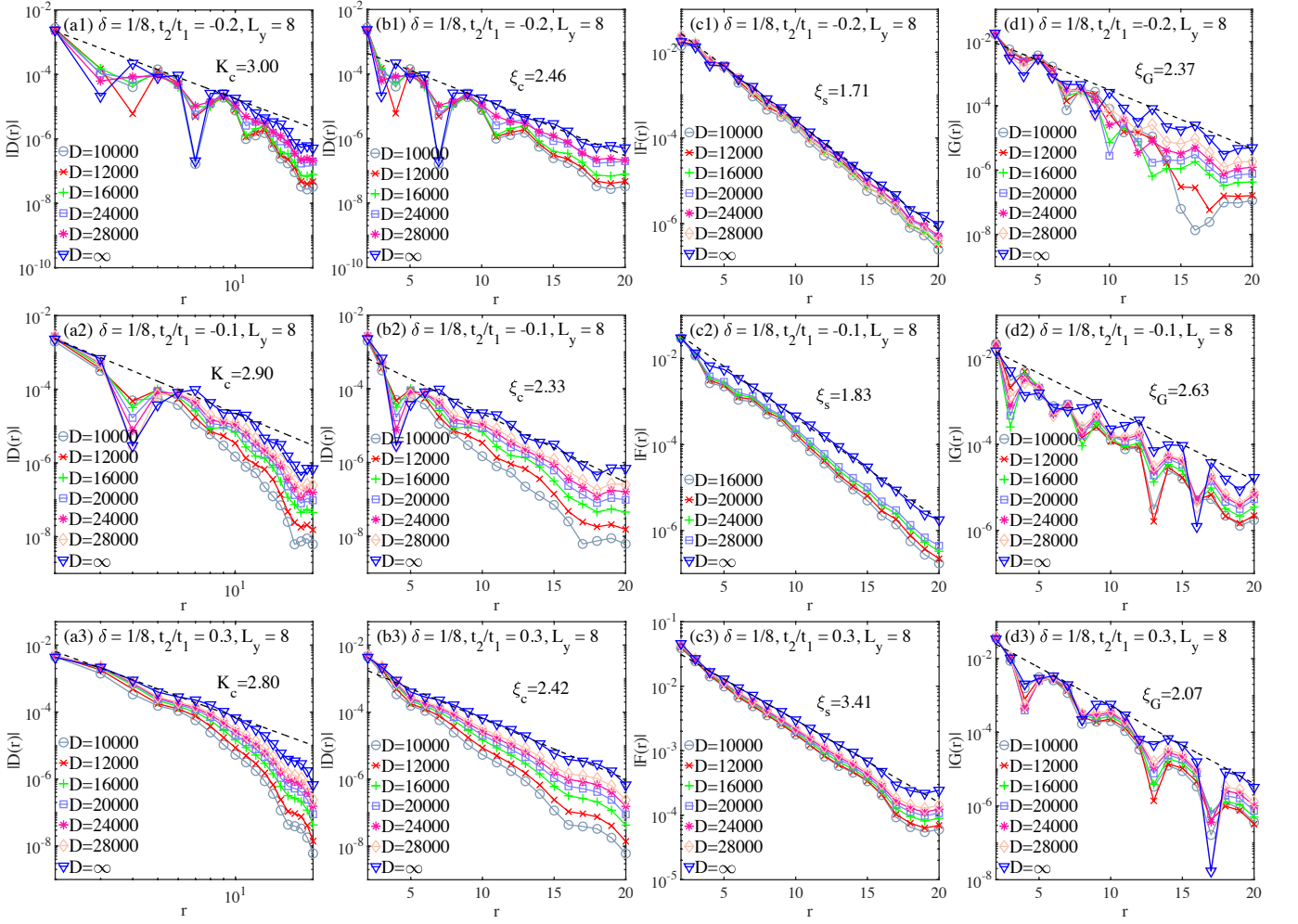


FIG. S2. **Scaling of the correlations in the SC and uniform d -wave SC phase on the $L_y = 8, L_x = 24$ cylinders.** (a1) and (b1) are respectively the double- and semi-logarithmic plots of charge density correlation $D(r)$ obtained by different bond dimensions in the SC phase ($\delta = 1/8, t_2/t_1 = -0.2$). (c1) and (d1) are the semi-logarithmic plots of spin correlation $F(r)$ and single-particle Green's function $G(r)$ in the same phase separately. The dashed line denotes the fitting of the extrapolated $D \rightarrow \infty$ results, where the corresponding power exponent K_c and correlation length ξ are obtained by fitting the algebraic behaviour $D(r) \sim r^{-K_c}$ and exponential behaviour $\sim \exp(-r/\xi)$. (a2-d2) and (a3-d3) are respectively the similar correlations in the SC phase ($\delta = 1/8, t_2/t_1 = -0.1$) and uniform d -wave SC phase ($\delta = 1/8, t_2/t_1 = 0.3$), respectively.

D. Charge density pattern and correlation functions in the W_y3 CDW phase

In this section, we discuss some properties of the W_y3 CDW phase. As we mentioned in the main text, the charge density distribution of the W_y3 CDW phase breaks the translational symmetry in the circumference direction with a period of 3, and the wavelength along the axis direction is $\lambda \simeq 2/(L_y\delta)$. To confirm this, we have performed simulations for different system lengths $L_x = 24 - 64$ that can match with the doping ratio, as shown in Fig. S7. One can find that with the increase of L_x , the distribution of charge density is always inhomogeneous in the y direction, suggesting that such an inhomogeneity may not be caused by the finite-size effect. In addition, we have also tried to keep larger bond dimensions and increase the number of sweeps, but the symmetry breaking in the y direction is not recovered. Therefore, we believe that this phase is a new kind of CDW phase carrying the wavevector $Q = (6\pi\delta, 2\pi/3)$.

We also find that such a charge density inhomogeneity in the W_y3 CDW phase usually suppresses the SC order. In Fig. S8(a), we compare different correlation functions and find that while the pairing correlation $P_{yy}(r)$ is the weakest, the charge density correlation is the strongest in the whole W_y3 CDW phase as expected. In Fig. S8(b), we also supplement with the comparison of pairing correlations in different phases on 6-leg cylinder. One can see that the $P_{yy}(r)$ are much weaker in W_y3 CDW phase with the power exponent $K_{sc} \gg 2$.

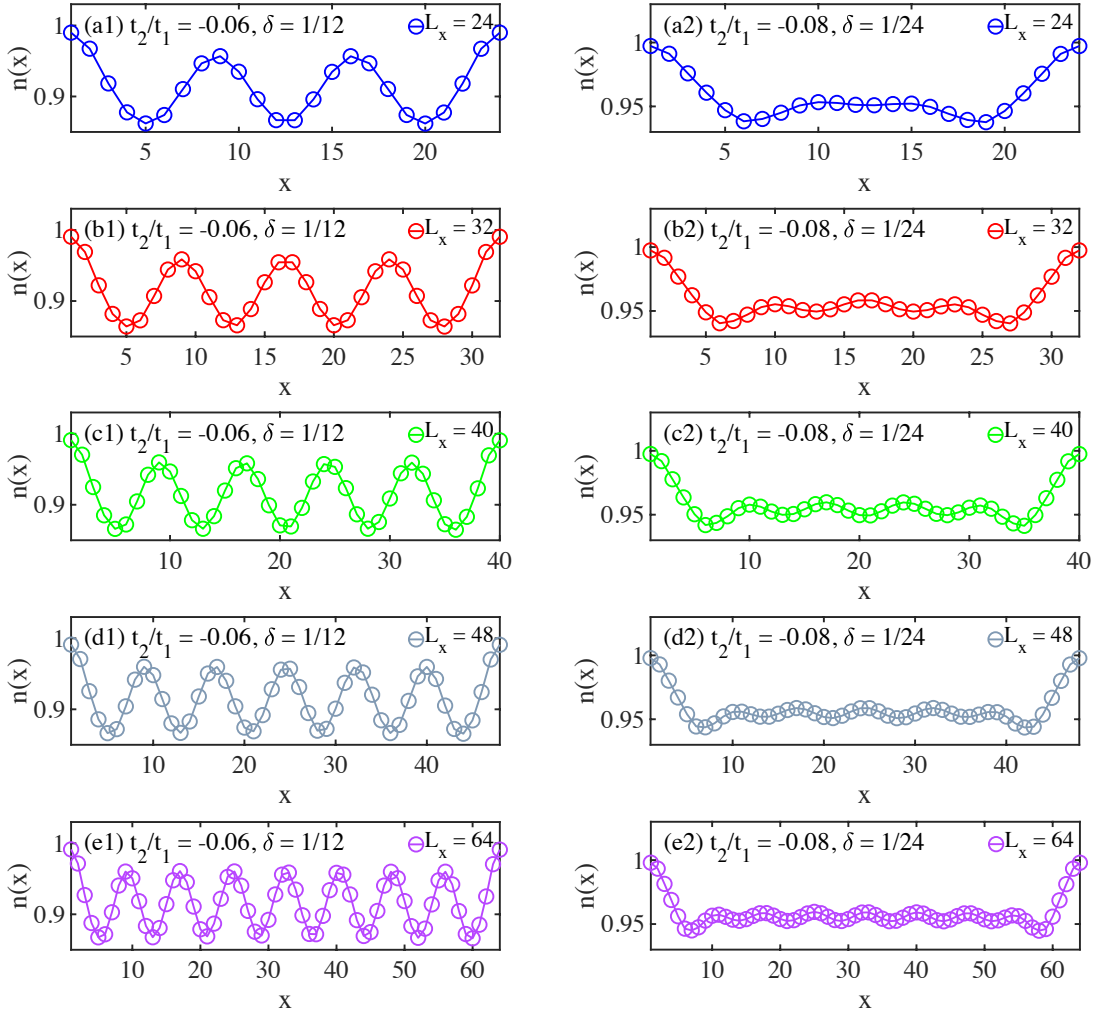


FIG. S3. **Charge density profiles on 6-leg cylinders.** Charge density profiles with different lattice sizes $L_x = 24 - 64$ in the stripe phase (a1-e1) and SC + CDW phase (a2-e2). Here, we select two representative parameters to show the charge density distributions of these two phases. The truncation error of all simulations are about $\mathcal{O}(10^{-6})$.

E. Static spin structure factor

In this section, we demonstrate the static spin structure factor $S(\mathbf{k})$ in different phases. For 6-leg cylinders [Fig. S9], generally speaking, the antiferromagnetic (AFM) correlation pattern are stronger at low doping levels and the peak at $\mathbf{k} = (\pi, \pi)$ splits gradually with the increase of doping level. In the stripe phase, $S(\mathbf{k})$ shows two round peaks around $\mathbf{k} = (\pi, \pi)$, and the momentum positions of the two peaks are related to the oscillations and π -phase shift of spin correlation, which is similar to the same phase at $t_2/t_1 > 0$ [41]. In the SC + CDW phase, although the peak at $\mathbf{k} = (\pi, \pi)$ is suppressed, the short-range AFM spin background persists and the peak does not split. However, in the W_y3 CDW phase, one can find that the spin correlation is short-ranged and $S(\mathbf{k})$ only has broad peaks around $\mathbf{k} = (\pi, \pi)$.

For 8-leg cylinders at $\delta = 1/8$ [Fig. S10], we find that $S(\mathbf{k})$ also has two peaks around $\mathbf{k} = (\pi, \pi)$ in the hole-doped SC phase [Fig. S10(a)], which is similar to the 6-leg $1/8$ doping system at larger $|t_2/t_1|$. In the uniform d -wave SC phase at $t_2/t_1 > 0$ [Fig. S10(b)], $S(\mathbf{k})$ shows a single peak at $\mathbf{k} = (\pi, \pi)$, consistent with the AFM correlation pattern in real space.

F. Electron momentum distribution

In Fig. S11, we provide the electron momentum distribution $n(\mathbf{k})$ for more parameters on 6-leg cylinders. One can find that the topology of the Fermi surface at $\mathbf{k} = (\pm\pi, 0)$ and $\mathbf{k} = (0, \pm\pi)$ is unenclosed in all the three phases at $t_2/t_1 < 0$, which

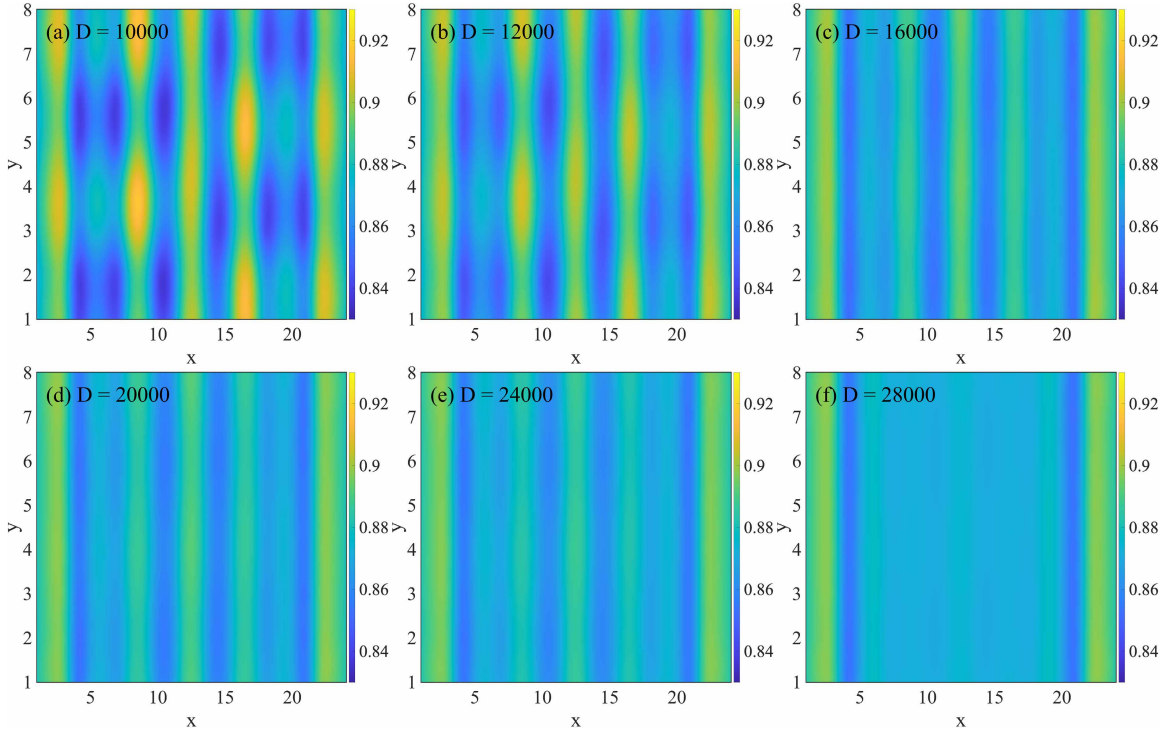


FIG. S4. **Bond dimension dependence of the charge density of all the sites in the hole-doped SC phase on 8-leg cylinder.** (a) to (f) correspond to the charge density distribution for $D = 10000$, $D = 12000$, $D = 16000$, $D = 20000$, $D = 24000$ and $D = 28000$, respectively. Here, we show the results of $\delta = 1/8$, $t_2/t_1 = -0.2$ on the $L_y = 8$, $L_x = 24$ cylinder.

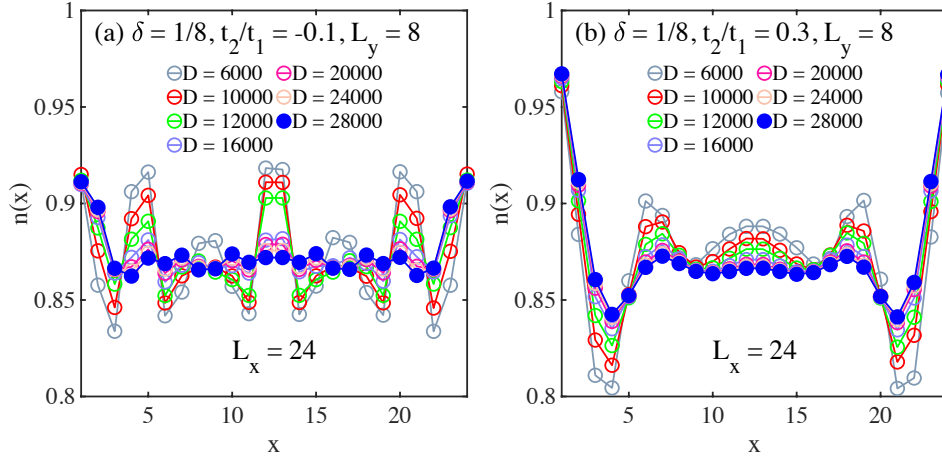


FIG. S5. **Bond dimension dependence of the charge density profiles on 8-leg cylinders.** (a) and (b) show the results on the $L_y = 8$, $L_x = 24$ cylinder at $\delta = 1/8$, for the hole-doped SC phase at $t_2/t_1 = -0.1$ and the uniform d -wave phase at $t_2/t_1 = 0.3$.

are consistent with the ARPES observation of hole-doped cuprates [58]. The same Fermi surface topology is also found on the 8-leg cylinder at $t_2/t_1 < 0$, $\delta = 1/8$ [Fig. S12(a)], which is in contrast to the electron-doped case [Fig. S12(b)], where the Fermi surface forms a closed pocket centered around $\mathbf{k} = (0, 0)$.

G. Extrapolation of correlation functions with growing bond dimension

In this section, we explain the bond dimension extrapolation process for correlation functions in more details. We perform polynomial extrapolations to best fit the data for a range of bond dimensions up to 15000 and 28000 SU(2) multiplets for 6- and

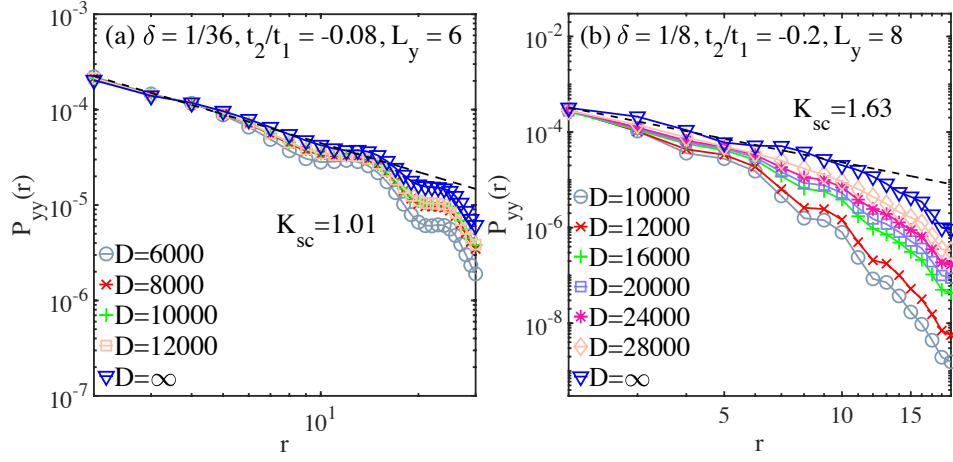


FIG. S6. **Scaling of pairing correlations for more parameter points in the superconducting phases.** (a) Double-logarithmic plot of $P_{yy}(r)$ at $\delta = 1/36, t_2/t_1 = -0.08$ on 6-leg cylinder, for the SC + CDW phase. The power exponent $K_{sc} \simeq 1.01$ is obtained by fitting $P_{yy}(r) \sim r^{-K_{sc}}$. The dashed line denotes the fitting of the extrapolated $D \rightarrow \infty$ results. (b) Similar plot of $P_{yy}(r)$ at $\delta = 1/8, t_2/t_1 = -0.2$ on 8-leg cylinders, for the hole-doped SC phase. The power exponent is obtained as $K_{sc} \simeq 1.63$.

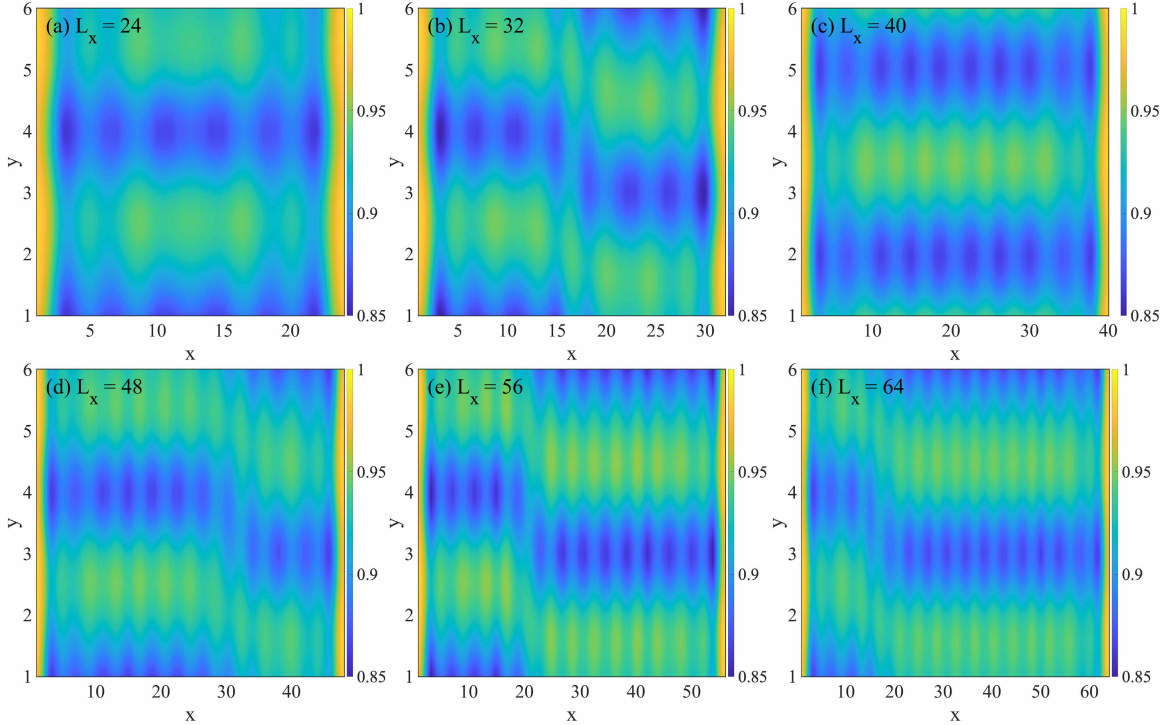


FIG. S7. **Charge density for all the lattice sites in the W_y3 CDW phase on 6-leg cylinders.** (a) to (f) correspond to the results for $L_x = 24, L_x = 32, L_x = 40, L_x = 48, L_x = 56$ and $L_x = 64$, respectively. Here, we show the data of $\delta = 1/12, t_2/t_1 = -0.2$ as a representative. The truncation error of all the simulations is about $\mathcal{O}(10^{-6})$.

8-leg cylinders. In Fig. S13, we show the extrapolations of the pairing correlations in the stripe phase (6-leg), SC + CDW phase (6-leg), SC phase (8-leg), and uniform d -wave phase (8-leg) as representative. For each given distance r , the correlations are extrapolated by the quadratic polynomial function $\mathcal{F}(1/D) = \mathcal{F}(0) + \alpha/D + \beta/D^2$ with five different bond dimensions. We have also checked that the cubic polynomial extrapolations give the similar results, which do not change the conclusions.

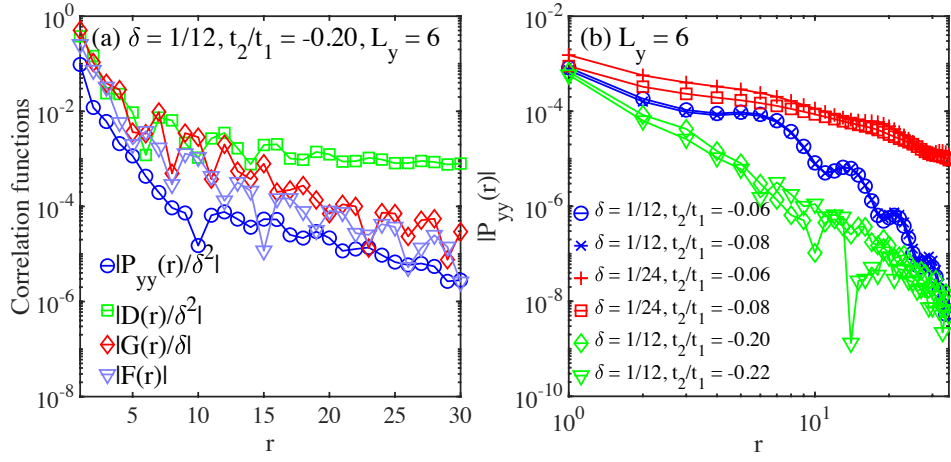


FIG. S8. **Correlation functions in the W_y3 CDW phase.** (a) Comparison among the pairing correlation $P_{yy}(r)$, charge density correlation $D(r)$, single-particle Green's function $G(r)$, and spin correlation $F(r)$ in the W_y3 CDW phase on 6-leg cylinders at $t_2/t_1 = -0.2$, $\delta = 1/12$. The correlations are rescaled by δ to make a direct comparison. (b) Double-logarithmic plot of $P_{yy}(r)$ for different t_2/t_1 at $\delta = 1/12$ and $\delta = 1/24$. Here we show the results obtained using the bond dimension $D = 15000$ on the $L_x = 48$ cylinder.

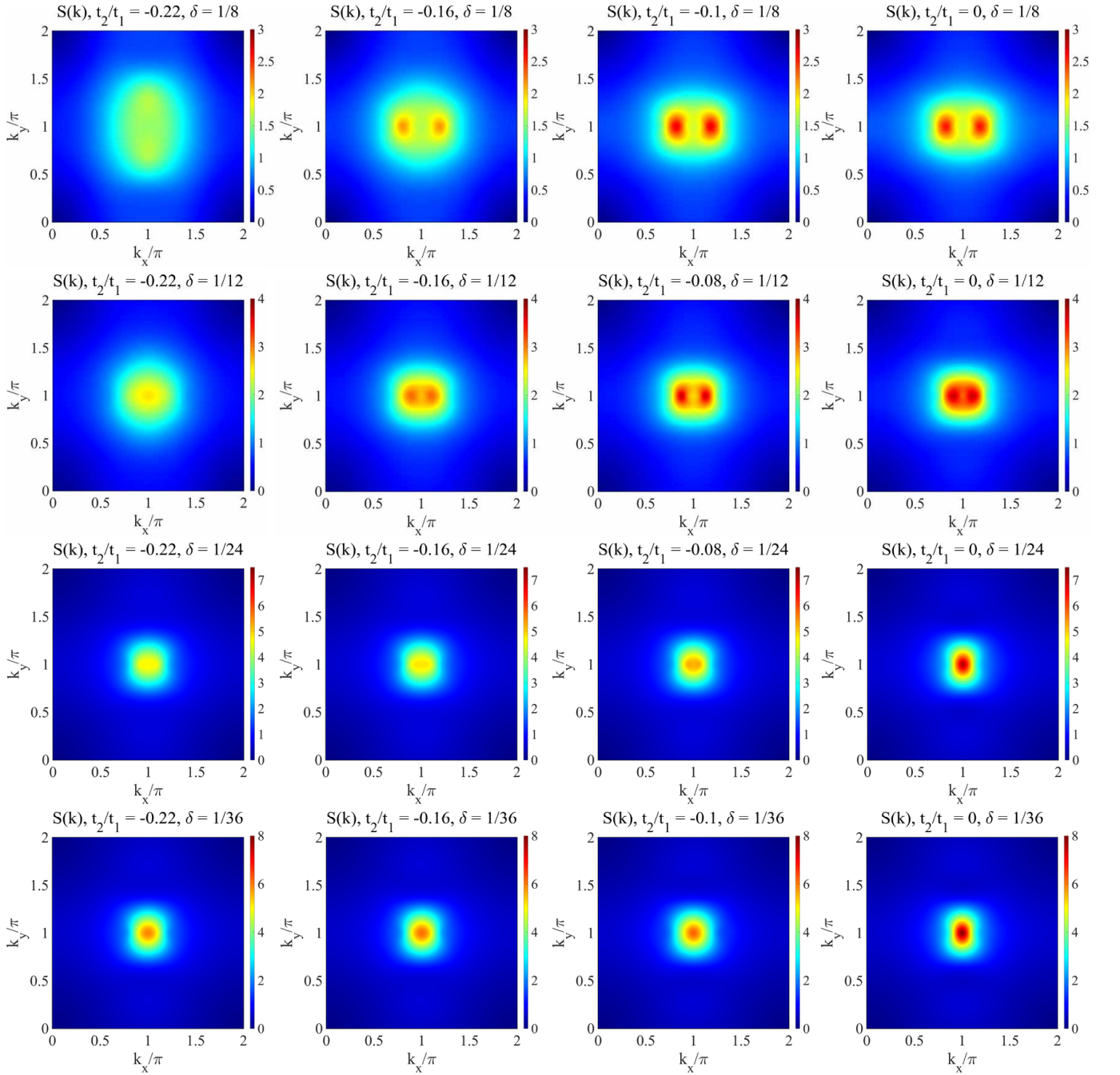


FIG. S9. **Static spin structure factors $S(\mathbf{k})$ for different t_2/t_1 and doping ratios δ on 6-leg cylinders.** $S(\mathbf{k})$ are obtained by taking the Fourier transformation for the spin correlations of the middle 32×6 sites on the 48×6 cylinders. In the stripe phase, $S(\mathbf{k})$ exhibits two round peaks around $\mathbf{k} = (\pi, \pi)$. While the single peak is well maintained in the SC + CDW phase. In the W_y3 CDW phase, $S(\mathbf{k})$ always show round peaks. All these measurements are obtained by keeping bond dimension $D = 12000$.

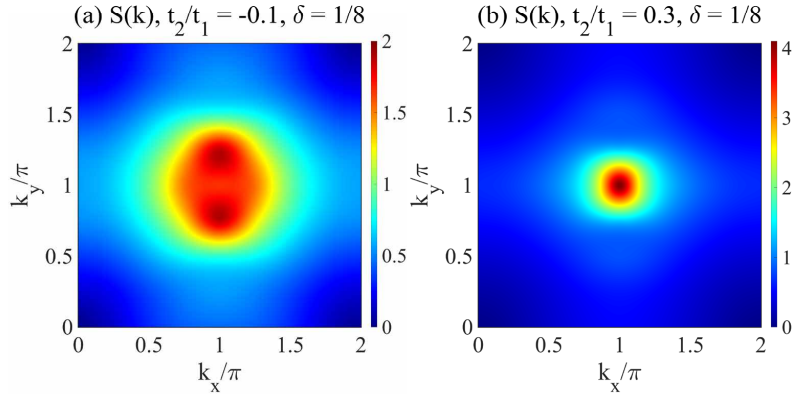


FIG. S10. **Static spin structure factors $S(\mathbf{k})$ for the hole-doped SC phase and uniform d -wave SC phase on 8-leg cylinders.** $S(\mathbf{k})$ are obtained by taking the Fourier transformation for the spin correlations of the middle 16×8 sites on the 24×8 cylinders. In the SC phase, there are two round peaks around $\mathbf{k} = (\pi, \pi)$, while a single peak in the uniform d -wave SC phase. All the measurements are obtained by keeping bond dimension $D = 16000$.

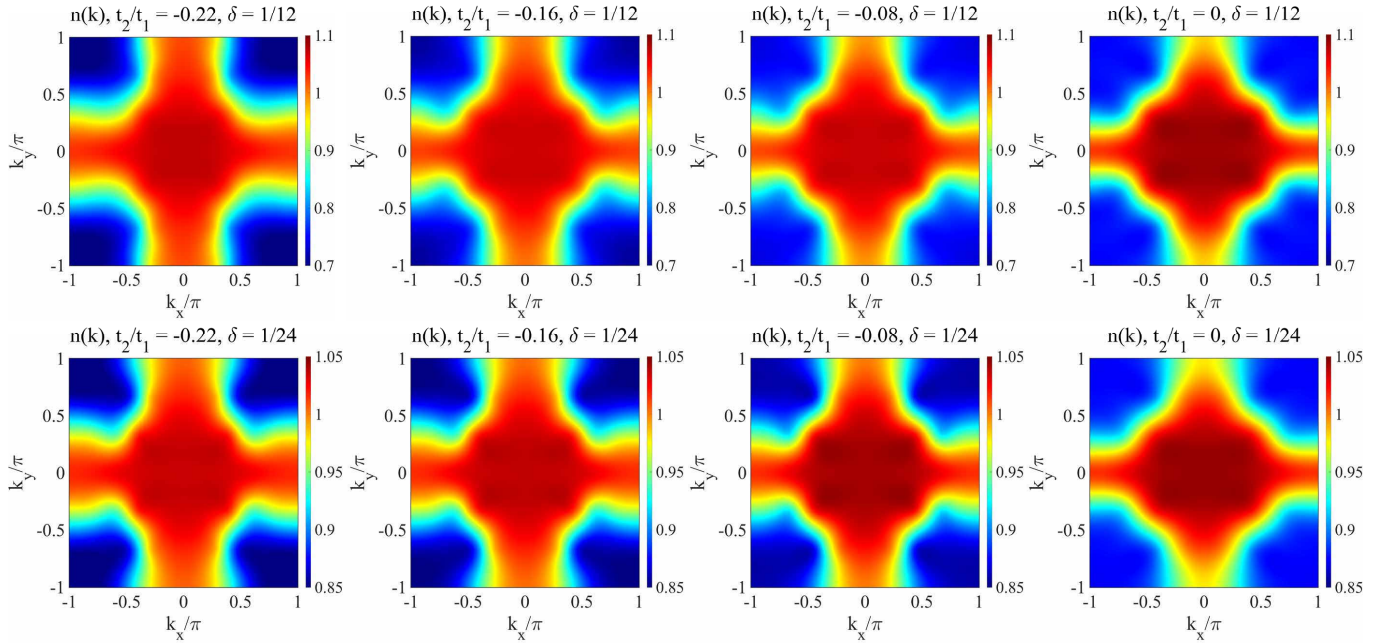


FIG. S11. **Momentum distribution functions $n(\mathbf{k})$ for different t_2/t_1 and doping ratios δ on 6-leg cylinders.** $n(\mathbf{k})$ are obtained by taking the Fourier transformation for the single-particle Green's functions of the middle 32×6 sites on the 48×6 cylinders. All the measurements are obtained by keeping bond dimension $D = 12000$.

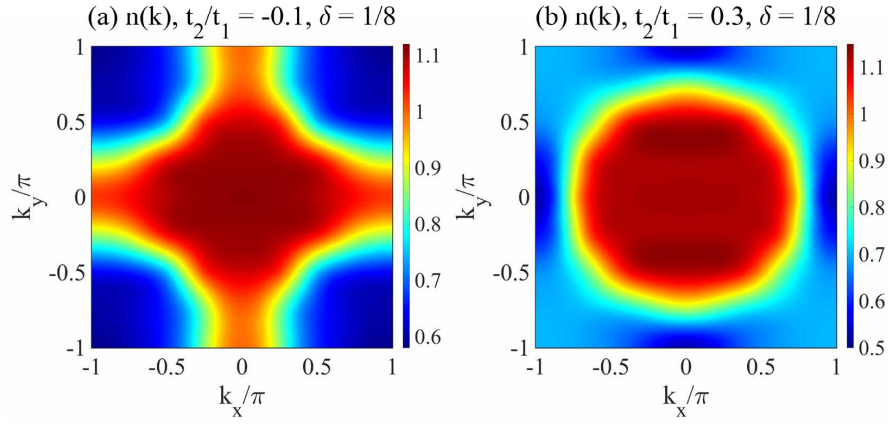


FIG. S12. **Momentum distribution functions $n(\mathbf{k})$ for the hole-doped SC phase and uniform d -wave SC phase on 8-leg cylinders.** $n(\mathbf{k})$ are obtained by taking the Fourier transformation for the single-particle Green's functions of the middle 16×8 sites on the 24×8 cylinders. All the measurements are obtained by keeping bond dimension $D = 16000$.

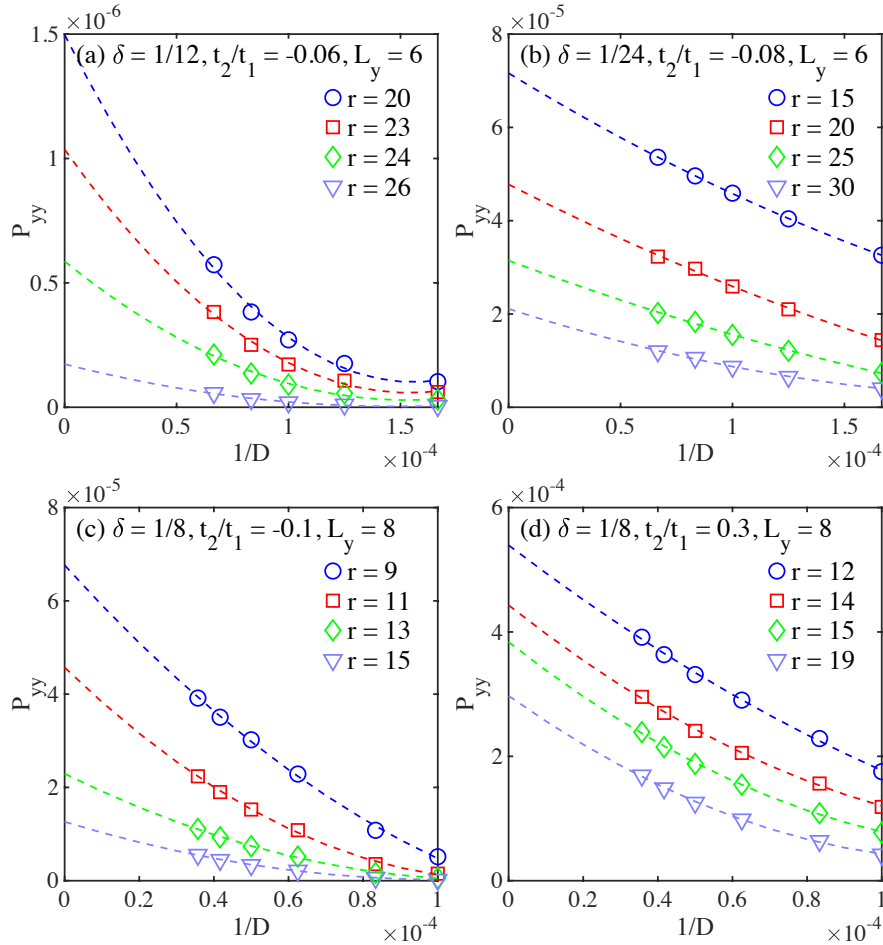


FIG. S13. **Extrapolations of correlation functions versus bond dimension.** (a) and (b) show the extrapolations of the pairing correlations P_{yy} on the 6-leg cylinders for $t_2/t_1 = -0.06$, $\delta = 1/12$ in the stripe phase, and $t_2/t_1 = -0.08$, $\delta = 1/24$ in the SC + CDW phase. D is the SU(2) bond dimension, which corresponds to $D = 6000, 8000, 10000, 12000, 15000$ here. (c) and (d) are the similar extrapolations on the 8-leg cylinders for $t_2/t_1 = -0.1$, $\delta = 1/8$ in the hole-doped SC phase, and $t_2/t_1 = 0.3$, $\delta = 1/8$ in the uniform d -wave SC phase. The kept bond dimensions correspond to $D = 10000, 12000, 16000, 20000, 24000, 28000$. The correlation data at each given distance r are extrapolated by the quadratic polynomial function $\mathcal{F}(1/D) = \mathcal{F}(0) + \alpha/D + \beta/D^2$.